Environmental Science & Technology

Article

pubs.acs.org/est

Mercury Deposition and Re-emission Pathways in Boreal Forest Soils Investigated with Hg Isotope Signatures

Martin Jiskra,*[,†,‡,⊥] Jan G. Wiederhold,*[,†,‡] Ulf Skyllberg,[§] Rose-Marie Kronberg,[§] Irka Hajdas,[∥] and Ruben Kretzschmar[†]

[†]Soil Chemistry Group, Institute of Biogeochemistry and Pollutant Dynamics, ETH Zurich, 8092 Zurich, Switzerland

[‡]Isotope Geochemistry Group, Institute of Geochemistry and Petrology, ETH Zurich, 8092 Zurich, Switzerland

[§]Department of Forest Ecology and Management, Swedish University of Agricultural Sciences (SLU), Skogmarksgränd, 90183 Umeå, Sweden

[∥]Laboratory of Ion Beam Physics, ETH Zurich, Otto-Stern-Weg 5, 8093 Zurich, Switzerland

Supporting Information

ABSTRACT: Soils comprise the largest terrestrial mercury (Hg) pool in exchange with the atmosphere. To predict how anthropogenic emissions affect global Hg cycling and eventually human Hg exposure, it is crucial to understand Hg deposition and re-emission of legacy Hg from soils. However, assessing Hg deposition and re-emission pathways remains difficult because of an insufficient understanding of the governing processes. We measured Hg stable isotope signatures of radiocarbon-dated boreal forest soils and modeled atmospheric Hg deposition and re-emission pathways and fluxes using a combined source and process tracing approach. Our results suggest that Hg in the soils was dominantly derived from deposition of litter (~90% on average). The remaining fraction was attributed to precipitation-derived Hg, which showed increasing contributions in older, deeper soil horizons (up to 27%) indicative of an accumulation over decades. We provide evidence for significant Hg re-emission from organic soil horizons most likely caused by nonphotochemical abiotic reduction by natural organic matter, a process previously not observed unambiguously in nature. Our data suggest that Histosols (peat soils), which exhibit at least seasonally water-saturated conditions, have re-emitted up to one-third of previously deposited Hg back to the atmosphere. Re-emission of legacy Hg following reduction by natural organic matter may therefore be an important pathway to be considered in global models, further supporting the need for a process-based assessment of land/atmosphere Hg exchange.

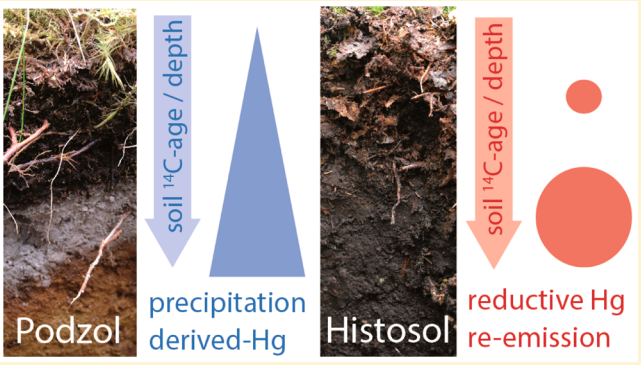

INTRODUCTION

Current global Hg models suggest that land surfaces receive 3200 Mg yr^{-1} through atmospheric deposition and re-emit 1700 to 2800 Mg yr^{-1},[1−3] illustrating the dual role of soils in global Hg cycling as sink and source for atmospheric Hg. After long-range transport, atmospheric Hg(0) is oxidized and deposited directly onto soils with precipitation or indirectly via plant surfaces with throughfall. Gaseous Hg(0) is also taken up through plant stomata, oxidized in the plants, and deposited onto soils with litterfall, or directly deposited from the atmosphere to terrestrial surfaces as dry deposition. In soils, Hg(II) may be methylated or reduced to volatile Hg(0) which is eventually re-emitted back to the atmosphere (Figure 1).[4] Several processes have experimentally been shown to reduce Hg(II): direct and indirect photochemical reduction, microbially mediated enzymatic reduction, and nonphotochemical abiotic reduction by minerals and natural organic matter (NOM).[5−11] However, their relative importance for reductive Hg loss from terrestrial ecosystems remains elusive. Quantitative estimates of Hg re-emission fluxes from terrestrial environments are scarce and suffer from considerable uncertainties due to large temporal and spatial variations in Hg fluxes and methodological limitations.[5] The establishment of Hg mass balances in soils remains challenging, because reliable estimates require knowledge of all Hg fluxes in parallel to total mass loss by carbon mineralization.[12,13] The difficulty of resolving gain and loss processes simultaneously was illustrated for instance by a litter decomposition study, in which a net Hg loss was observed in the absence of additional Hg input in the laboratory, whereas a net Hg accumulation was found for the same set of samples under field conditions.[14]

Received: February 10, 2015
Revised: April 28, 2015
Accepted: May 6, 2015
Published: May 6, 2015

DOI: 10.1021/acs.est.5b00742
Environ. Sci. Technol. 2015, 49, 7188−7196

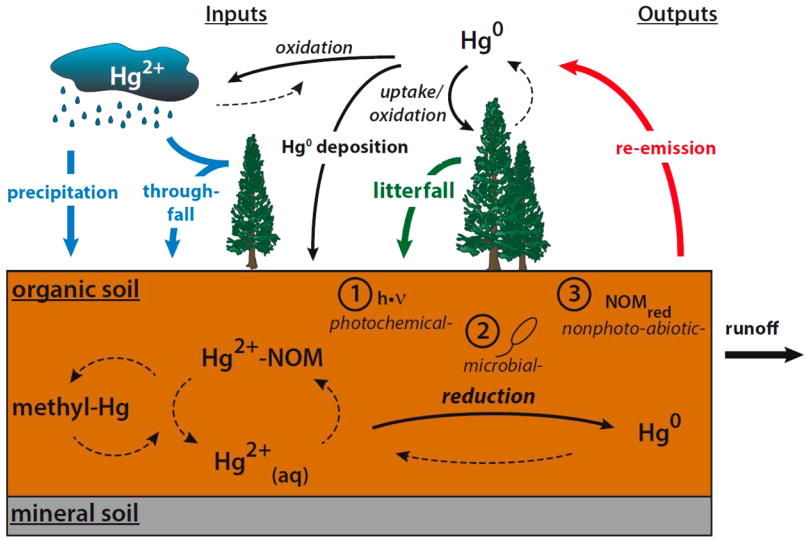

Figure 1. Conceptual model of the terrestrial Hg cycle: Major input and output pathways. Atmospheric Hg is mainly deposited as oxidized Hg(II) via precipitation and throughfall or taken up by plant stomata and deposited with litterfall. In soils, Hg(II) can be reduced by different pathways: (1) photochemical, (2) microbial, or (3) nonphotochemical abiotic reduction by natural organic matter (NOM), followed by re-emission back to the atmosphere. All Hg forms are subjected to leaching from soils with surface or subsurface runoff into aquatic ecosystems.

Stable Hg isotope analyses offer a new approach for identifying different Hg sources and processes through characteristic mass-dependent (MDF) and mass-independent (MIF) fractionation of Hg isotopes associated with each source and reduction pathway.[15] On the one hand, distinct differences in isotope signatures of Hg in precipitation, atmospheric Hg(0), and Hg in litter allow tracing the different pathways of atmospheric Hg deposition to terrestrial ecosystems.[16,17] On the other hand, different biogeochemical reactions, in particular reduction processes, have been experimentally shown to be associated with characteristic Hg isotope fractionation trajectories offering the potential to gain information on reduction pathways in terrestrial samples. Photochemical reduction of Hg(II) favors light isotopes leading to MDF and is associated with large MIF by magnetic isotope effects (MIE).[11,18,19] Microbial reduction also favors light Hg isotopes, but without MIF.[10] NOM in the absence of sunlight preferentially reduces light Hg isotopes and exhibits MIF caused by nuclear volume fractionation (NVF).[9]

In this study, we measured the Hg isotope composition of boreal forest soils in Northern Sweden in combination with radiocarbon dating of the soil NOM to address the following objectives: (i) to assess the pathways of Hg deposition to boreal forest soils, and (ii) to investigate the reduction pathways and quantify reductive Hg losses and re-emission fluxes from boreal forest soils.

MATERIALS AND METHODS

Soil Samples. Two major soil types, Podzols and Histosols, both characteristic for boreal forest ecosystems, were investigated. Podzols are acidic soils, encompassing different layers of slowly decomposing NOM (O horizons) overlying the diagnostic mineral E and B horizons, that typically develop in more well-drained landscape positions. Histosols (peat soils) are organic soils having a thickness of more than 40 cm (H horizons) and commonly form by net accumulation of NOM under water-saturated conditions. In managed forests, Histosols are often partly drained remains of former wetlands or riparian zones along streams and ditches. Podzols cover ~15% and Histosols ~7% of the northern circumpolar region.[20] Soil samples were collected in a remote area north of the town Junsele in northern Sweden (N:63°50′, E:17°00′) from two typical boreal Norway spruce (>80 years old) forest stands (see map in Supporting Information, SI, Figure S1). The area is covered by glacial till originating from gneissic/granitic bedrock and has a cold-humid climate. It receives an average annual precipitation of 530 mm and has a mean temperature of 2 °C (Jan: −11 °C, Jul: 15 °C, 1961−1990, Swedish Meteorological Institute, SMHI). All sampling locations were situated in two forest stands within an area of ~1 km^2, we therefore assume that all soils were exposed to the same source and amount of atmospheric Hg deposition. The soil samples were separated into the organic surface horizons (Oe/He) after removal of living mosses and loose litter, the underlying Oa/Ha horizons comprised by older more decomposed NOM, and for Podzols the mineral horizons (E+B). Composite samples (5 subsamples within 10 m^2) were taken from several transects, each starting near a small stream and following the inclination of the landscape uphill along a slope, thereby covering a range of hydrological conditions. Litter samples were collected after snowmelt as composite samples from the soil surface (>25 subsamples within 100 m^2) at four different locations, two on Podzols and Histosols, respectively. All litter samples were similar in composition, mainly consisting of *Picea abies* needles and remains from the predominant dwarf shrubs (*Vaccinium myrtillus*, *Empetrum nigrum*, and *Calluna vulgaris*). The soil sampling and sample processing scheme is further described in the SI.

Analytical Methods. For stable Hg isotope measurements, soil samples were combusted in a two-step oven system coupled to an oxidizing liquid trap (1% $KMnO_4$). The Hg recovery was 94% ± 8.5% (1σ, n = 72) and process blanks run after every 10 samples contained 0.04 ± 0.01 ng mL^{-1} Hg (1σ, n = 9), corresponding to less than 1% of total concentrations in samples. The Hg isotope composition of the trap solutions was measured using cold vapor multicollector inductively coupled plasma mass spectrometry (CV-MC-ICPMS) employing sample-standard bracketing and Tl addition for mass bias

DOI: 10.1021/acs.est.5b00742
Environ. Sci. Technol. 2015, 49, 7188−7196

correction, following previously developed methods[21] (see SI for details). Hg isotope data are reported relative to NIST-3133 for MDF as follows:

$$\delta^{202}\mathrm{Hg} = \frac{(^{202}\mathrm{Hg}/^{198}\mathrm{Hg})_{\mathrm{sample}}}{(^{202}\mathrm{Hg}/^{198}\mathrm{Hg})_{\mathrm{NIST\text{-}3133}}} - 1 \quad (1)$$

and for MIF as follows:

$$\Delta^{199}\mathrm{Hg} = \delta^{199}\mathrm{Hg} - (\delta^{202}\mathrm{Hg} \times 0.2520) \quad (2)$$

$$\Delta^{200}\mathrm{Hg} = \delta^{200}\mathrm{Hg} - (\delta^{202}\mathrm{Hg} \times 0.5024) \quad (3)$$

$$\Delta^{201}\mathrm{Hg} = \delta^{201}\mathrm{Hg} - (\delta^{202}\mathrm{Hg} \times 0.7520) \quad (4)$$

Isotopic differences in MDF between different pools are defined as

$$\varepsilon^{202}\mathrm{Hg}_{\mathrm{pool1-pool2}} = \delta^{202}\mathrm{Hg}_{\mathrm{pool1}} - \delta^{202}\mathrm{Hg}_{\mathrm{pool2}} \quad (5)$$

Isotopic differences in MIF between different pools are defined as follows:

$$\mathrm{E}^{xxx}\mathrm{Hg}_{\mathrm{pool1-pool2}} = \Delta^{xxx}\mathrm{Hg}_{\mathrm{pool1}} - \Delta^{xxx}\mathrm{Hg}_{\mathrm{pool2}} \quad (6)$$

where ^{xxx}Hg corresponds to ^{199}Hg, ^{200}Hg, or ^{201}Hg.

The isotopic enrichment factor is defined as follows:

$$\varepsilon^{202}\mathrm{Hg}_{\mathrm{product/reactant}} = \alpha^{202}\mathrm{Hg}_{\mathrm{product/reactant}} - 1 \quad (7)$$

with $\alpha^{202}\mathrm{Hg}_{\mathrm{product/reactant}}$ representing the fractionation factor reported in the corresponding publications (SI Table S4).[9−11] Our in-house standard (ETH-Fluka) was measured regularly and had a reproducibility of δ^{202}Hg = −1.44 ± 0.11‰, Δ^{199}Hg = 0.07 ± 0.05‰, Δ^{200}Hg = 0.01 ± 0.06‰, and Δ^{201}Hg = 0.03 ± 0.06‰ (2σ, n = 21) in agreement with previously measured values.[21−24] A process standard (Montana Soil, NIST-2711) was combusted in the oven system after every 10 samples and reproduced at δ^{202}Hg = −0.12 ± 0.10‰, Δ^{199}Hg = −0.23 ± 0.07‰, Δ^{200}Hg = 0.00 ± 0.04‰ and Δ^{201}Hg = −0.18 ± 0.02‰ (2σ, n = 10), consistent with previously published values.[22,23,25] Isotope measurements of peat samples low in ambient Hg and spiked with inorganic Hg(II) were in agreement with separate measurements of the inorganic Hg(II),[21] confirming the accuracy of our method for matrices prevalent in organic topsoils.

Radiocarbon Dating. Homogenized samples of bulk soil were combusted, graphitized and analyzed using Accelerator Mass Spectrometry (AMS; ETH Zurich).[26] ^{14}C data are reported as fraction of modern ^{14}C (F^{14}C), that is, concentration of ^{14}C normalized to the standard and corrected for mass fractionation using δ^{13}C. Radiocarbon ages are reported according to Stuiver and Polach[27] and for samples containing postbomb carbon the F^{14}C is reported according to Reimer et al.[28] Calibrations of the radiocarbon data were performed using the OxCal software (version 4.2.3, Bronk Ramsey, 2013). All prebomb carbon data (F^{14}C <1) were calibrated using the IntCal13 atmospheric ^{14}C curve.[29] Samples with F^{14}C >1 were calibrated using the postbomb NH1 atmospheric ^{14}C curve.[30] It is important to note that carbon in the soil samples represents a mixture of old and young carbon, therefore the interpretation of a bulk age should be used with caution.

Hg Isotope Model. Hg in soils is derived from geogenic origin or from atmospheric deposition, which can be further separated into wet deposition (precipitation and throughfall), litterfall, and dry deposition. For the Hg isotope mixing model used in this study, the atmospheric Hg deposition was described by two endmembers with distinct Hg isotope signatures: litter-derived and precipitation-derived Hg. Litter-derived Hg was defined based on the four litter composite samples collected on the forest floor of the study site. The Hg isotope signature in litter thus integrates the processes taking place in the canopy and potential uptake of wet deposition during snowmelt and therefore represents a robust endmember for the start of pedogenesis as indicated by the similar Hg isotope signatures of litter and Podzol Oe samples (see Results and Discussion). However, this approach does not allow resolving the entire complexity of atmospheric deposition.

We modeled the endmember of precipitation-derived Hg using previously published precipitation data,[16,31−34] measured across North America (see SI), based on the assumption that the Hg isotope composition of precipitation is globally uniform. Measurements of Hg in precipitation at our sampling site were unfortunately not available. Consistent Hg isotope signatures of atmospheric Hg(0) have been reported for North America[16,19,31] and Europe.[35] Recently published precipitation data from China[36] and preliminary precipitation data from France, Europe (J. Sonke, personal communication) are in agreement with the published values from North America. Therefore, we consider these values to be a reasonable estimate for the precipitation endmember at our field site as well.

In previous Hg isotope source tracing studies in soils, geogenic Hg was used as an additional Hg source in mixing calculations.[16,17] We estimated the content of mineral material in the organic topsoils from the measured Si concentration in each sample, assuming a SiO_2 concentration of 60% (w/w) for granite, the predominant bedrock in the sampling area. Alriksson et al.[37] reported an average Hg concentration of 13 ng g^{-1} (SE = ± 0.7 ng g^{-1}, n= 200) for mineral C horizons in Sweden. Using this value as a conservative estimate (probably overestimated due to atmospheric influence) for the geogenic background Hg concentration, its contribution to the total Hg in the samples was calculated to be on average 0.36% (maximum 1.8%). The Hg isotope composition previously reported for rocks has shown no significant MIF and also the variation in MDF was limited.[38] Therefore, we conclude that the contribution of Hg from geogenic origin can be considered negligible in the organic topsoils of this study and thus we did not incorporate a geogenic endmember in the mixing scenarios.

The source contributions and reductive losses in boreal forest soil samples were modeled by a Monte Carlo simulation approach, using the pseudorandom number generation function of the Matlab software (R2012a, MathWorks). The model consisted of two source components (litter- and precipitation-derived Hg) and a reductive loss component incorporating MDF (δ^{202}Hg) and MIF (Δ^{199}Hg, Δ^{200}Hg, and Δ^{201}Hg). The mixing endmembers were described based on the average and variance of the four measured litter samples (SI Table S3) and the average and variance of previously published precipitation data[16,31−34] (SI Table S2) and atmospheric Hg(0) data[35] (SI Table S3). For Hg isotope signatures of soil samples which could not be described by a mixing of precipitation- and litter-derived Hg, results from the model including reductive Hg loss are reported. Experimental fractionation factors for nonphotochemical abiotic NOM reduction[9] and microbial reduction[10] were used for reductive loss estimations (SI Table S4). Median model parameters for fraction precipitation ($f_{\mathrm{precipitation}}$) and fraction of reductive loss (f_{reduced}) with the

DOI: 10.1021/acs.est.5b00742
Environ. Sci. Technol. 2015, 49, 7188−7196

corresponding standard deviation are reported. Further information on the modeling approach and the mixing component scenarios is provided in the SI.

Hg Re-emission Flux Calculation. The Hg pool (Hg_{pool}, $\mu g\ m^{-2}$) for each horizon was calculated using the Hg concentration, horizon thickness, and soil bulk density. Using the modeled reductive loss ($f_{reduced}$) and mean age of the soil carbon (calibrated ^{14}C-age, yr) we calculated the re-emission fluxes ($F_{re-emission}$, $\mu g\ m^{-2}\ yr^{-1}$) for each horizon:

$$F_{re-emission} = \frac{(1 + f_{reduced}) \times Hg_{pool} \times f_{reduced}}{\text{calibrated } ^{14}\text{Cage}} \quad (8)$$

The overall re-emission flux was calculated from the sum of the organic horizons. On the basis of recent observations suggesting that mineral soil horizons might be net sinks for gaseous Hg(0),[39] reductive re-emission from mineral horizons was not considered.

RESULTS AND DISCUSSION

Hg Isotope Signatures of Boreal Forest Soils. All soil and litter samples exhibited Hg concentrations in the range of 17 to 313 ng g^{-1} and negative MDF ($\delta^{202}Hg$ = −2.56‰ to −1.55‰) and MIF ($\Delta^{199}Hg$ = −0.48‰ to −0.24‰) signatures (n = 26) consistent with previously reported soil and litter data.[16,17,40] Litter samples exhibited the most negative MDF ($\delta^{202}Hg$ = −2.35 ± 0.09‰) and MIF ($\Delta^{199}Hg$ = −0.44 ± 0.03‰) (Figure 2). Relative to the average global

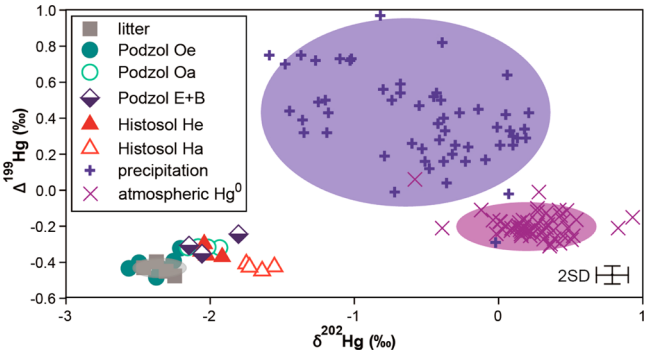

Figure 2. Mass-independent fractionation ($\Delta^{199}Hg$) vs mass-dependent fractionation ($\delta^{202}Hg$) signatures in boreal litter and soil samples (this study) and in previously published data for precipitation[16,31−34] and atmospheric Hg(0)[16,19,31,35] with the filled shapes representing 5- to 95-percentiles.

atmospheric Hg(0) isotope signature ($\delta^{202}Hg$ = 0.24 ± 0.24‰, $\Delta^{199}Hg$ = −0.19 ± 0.06‰) based on published results,[16,19,31,35] the litter samples were enriched in light Hg isotopes ($\varepsilon^{202}Hg_{litter-Hg(0)atm.}$ = −2.59 ± 0.25‰) and depleted in odd mass isotopes ($E^{199}Hg_{litter-Hg(0)atm.}$ = −0.24 ± 0.07‰). This is in agreement with observations by Demers et al.,[16] who reported a large enrichment of light Hg isotopes in tree foliage relative to atmospheric Hg^0 ($\varepsilon^{202}Hg_{litter-Hg(0)atm.}$= −2.89‰). The Podzol Oe horizons were characterized by similar $\delta^{202}Hg$ and $\Delta^{199}Hg$ values as the litter samples. Compared to the surface organic horizons of both Podzols and Histosols (Oe/He), the underlying Oa/Ha horizons were enriched in heavy isotopes ($\varepsilon^{202}Hg_{Oa-Oe}$= 0.37‰, p < 0.02 and $\varepsilon^{202}Hg_{Ha-He}$= 0.34‰, p < 0.001, t test) (Figure 3). Podzol Oa horizons exhibited positive MIF enrichment ($E^{199}Hg_{Oa-Oe}$= 0.11‰, p < 0.001, t test), whereas Histosol Ha horizons showed negative MIF enrichment ($E^{199}Hg_{Ha-He}$= −0.08‰, p < 0.02, t test) when compared to the overlying Oe and He horizons, respectively.

Hg Deposition Pathways. The results from the mixing model suggested that litter-derived Hg was by far the dominant source (average: 90%, 70−99%) for all Histosol and Podzol samples, with the remaining fraction (average: 10%) attributed to precipitation-derived Hg (Figure 3). These results are in agreement with previous estimates based on isotope measurements in Wisconsin, U.S.A., where precipitation-derived Hg accounted for 16% of the Hg reaching soils in a forested ecosystem.[16] Some previous concentration-based estimates however suggested higher contributions of precipitation-derived Hg deposition.[12,13,41] Demers et al.[16] suggested that this discrepancy between isotope and concentration based model approaches may be explained by throughfall having a Hg isotope composition similar to that of litterfall. Throughfall, by inclusion of dry deposition, undoubtedly provides an important source for soil Hg[42,43] that may have another isotopic composition than open field precipitation. However, since its Hg isotope signature is currently unknown, further investigations are needed before it can be used as a potential model input in future studies.

The modeled fraction of precipitation-derived Hg relative to total Hg increased in Podzols with soil depth from Oe (5% ± 4%), to Oa (16% ± 3%), and E+B (20% ± 9%) horizons (SI Table S9, no reduction). The calibrated radiocarbon ages in Podzols ranged from ∼10 years in litter to ∼60 to 120 years in E+B horizons (Figure 4, SI Table S7). The positive correlation observed between the modeled $f_{precipitation}$ and the radiocarbon signature in Podzols ($F^{14}C$, R^2 = 0.81, p < 0.001, SI Figure S9c) suggests that precipitation-derived Hg is transported vertically through the topsoil and is accumulated in lower Oa and mineral horizons over time scales of decades. Obrist et al.[44] recently proposed a time-dependent increase in Hg concentrations in soils and litter based on elemental ratios and suggested the accumulation of precipitation-derived Hg over time and/or mass loss through carbon mineralization as possible causes. The results from the boreal Podzols studied here suggest that the accumulation of precipitation-derived Hg over time accounted for ∼10% of the increase in Hg concentration, with the remaining fraction attributed to carbon mineralization and higher atmospheric Hg deposition at the time of deeper soil horizon formation. Histosol samples with calibrated radiocarbon ages between ∼20 years up to ∼1000 years exhibited relatively constant $f_{precipitation}$ of 12% ± 2% for He, and 10% ± 2% for Ha and did not follow time-dependent trends (SI Table S10, NOM reduction). This may be explained by the hydrological conditions in Histosols, in which water saturation is expected to seasonally hinder vertical transport.[45,46] None of the measured soil samples exhibited even-mass Hg isotope anomalies ($\Delta^{200}Hg$) outside analytical uncertainty, in contrast to all precipitation measurements published so far,[16,31−34] which is further support for a relatively small contribution of precipitation-derived Hg in soils.

Reductive Hg Re-emission Pathways. Some observed Hg isotope signatures from the Histosols (all four samples from the Ha horizon and one from the He horizon) could not be explained by simple litter/precipitation endmember mixing (blue area in Figure 3) and thus provided evidence for secondary processes or possibly the influence of additional Hg sources. A contribution from the isotopic signal of atmospheric Hg(0) in dry deposition, previously shown to be associated

DOI: 10.1021/acs.est.5b00742
Environ. Sci. Technol. 2015, 49, 7188−7196

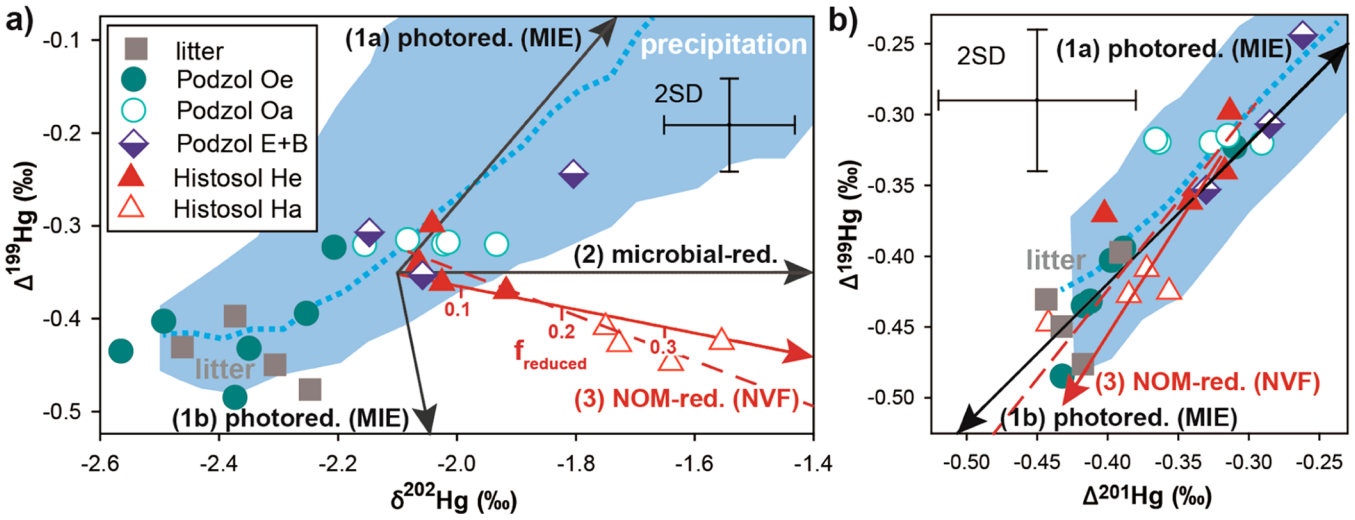

Figure 3. (a) Mass-independent fractionation (Δ^{199}Hg) vs mass-dependent fractionation (δ^{202}Hg) and (b) mass-independent fractionations Δ^{199}Hg vs Δ^{201}Hg in boreal litter and soil samples. The blue area represents the 5- to 95-percentile interval of mixing scenarios for litter- and precipitation-derived Hg (dotted line = median). The arrows represent the trajectories for photochemical reduction (photored.) in the presence of DOC (1a)[11] and in snow (1b),[19] microbial reduction (2),[10] and nonphotochemical abiotic reduction by natural organic matter (NOM-red.) (3)[9] with the respective amount of reductive loss ($f_{reduced}$). The linear regressions for the Histosol samples discussed in the text are illustrated by dashed lines. Note that each data point represents a composite sample taken from an area of about 10 m^2 (soils) and 100 m^2 (litter).

with negative Δ^{199}Hg values,[16,19,31,35] could theoretically explain the low Δ^{199}Hg in the Histosol Ha samples. However, mixing scenarios involving atmospheric Hg(0) dry deposition as additional source would require very low contributions of precipitation-derived Hg (SI Table S10). Furthermore, it can be assumed that the Hg isotope signatures in the Histosol Ha samples have evolved from the signatures observed in the overlying Histosol He samples. Since the addition of atmospheric Hg(0) to the signatures of the He samples could not explain the Hg isotope variation observed in the Ha samples, an important influence of atmospheric Hg^0 dry deposition appears to be unlikely.

Different Hg(II) reduction pathways have been shown experimentally to be associated with distinct Hg isotope fractionation trajectories (Figure 3). Photochemical Hg reduction, potentially active in foliage[16,42] and in the forest floor, has a fractionation trajectory toward the isotope signature of precipitation-derived Hg (Figure 3: (1a)[11]) and would lead to an overestimation of $f_{precipitation}$ in the mixing calculation. The fractionation trajectory of photochemical Hg reduction in snow (Figure 3: (1b)[19]) would lead to negative Δ^{199}Hg signatures, however the depletion in odd Hg isotopes ($E^{199}Hg_{Ha-He}$= −0.08‰) together with the observed MDF trend ($\varepsilon^{202}Hg_{Ha-He}$= 0.34‰) could not be explained by a combination of photochemical reduction processes alone.

The fractionation trajectory of direct microbial reduction (Figure 3: (2)), considered to be an important Hg reduction pathway in natural systems,[47,48] is similar to that of NOM reduction (Figure 3: (3)), except for the lack of MIF. Model simulations involving microbial reduction as a secondary process were able to explain the signatures of most of the Histosol Ha samples, but only in combination with high reductive losses (~70%) and low contributions of precipitation-derived Hg (~6%) (SI Table S9). However, this requires that the initial Hg concentrations would have been unreasonably high (~850 ng g^{-1}) and that the contribution of precipitation-derived Hg in the Histosol Ha samples would have been significantly lower compared with the overlying He samples, contrary to the expected trend with depth. Therefore, we suggest that the Hg isotope variation observed in Histosol Ha samples was not controlled by reductive loss through microbial reduction alone.

The linear regression of the Histosol Δ^{199}Hg vs δ^{202}Hg data revealed a significant negative slope of −0.24, (Figure 3a, 95% confidence interval: −0.09 to −0.40, p = 0.044, n = 8), which agreed well with the trajectory for NOM-driven Hg(II) reduction (3).[9] The Δ^{199}Hg/Δ^{201}Hg ratio of all soil samples was 1.02 ± 0.13, consistent with previously reported data for soils[16,17,38,40] and likely dominated by MIE of photochemical reactions prior to atmospheric deposition, which is expected to fractionate with a ratio of Δ^{199}Hg/Δ^{201}Hg = 1.[11,19] MIF during NOM-driven Hg(II) reduction, caused by NVF, is expected to fractionate the odd-mass isotopes in a ratio of Δ^{199}Hg/Δ^{201}Hg = 1.6.[9,49] The linear regression analysis of the Histosol samples, incorporating residues on Δ^{199}Hg as well as Δ^{201}Hg,[50] indicated an average Δ^{199}Hg/Δ^{201}Hg slope of 1.25 (Figure 3b, 95% confidence interval: 0.26 to 2.25, p = 0.044, n = 8). This is in agreement with the slope expected from NVF, the quality of the regression however did not allow a conclusive mechanistic determination based on the Δ^{199}Hg/Δ^{201}Hg ratio.

Another process potentially causing Hg isotope fractionation in organic soil horizons is sorption of Hg(II) to NOM.[49] However, since in principle all Hg is bound to NOM functional groups, we expect only very small net isotope effects from sorption. In line with this, we observed no Hg isotope fractionation between soil horizons and corresponding creek runoff in an ongoing study from the same study area.[46] Mercury methylation and demethylation processes were also not able to affect the bulk Hg isotopic composition, as methyl-Hg levels were low (≤1.3% of Hg_{tot}, SI). Reoxidation of Hg(0) could potentially cause significant Hg isotope fractionation, but this has not yet been investigated.

Little is known about the temporal variation of Hg isotope signatures in atmospheric Hg(0) and precipitation, thus the Hg isotope composition of the atmospheric sources was assumed to be constant. The amount of atmospheric Hg deposition was

DOI: 10.1021/acs.est.5b00742
Environ. Sci. Technol. 2015, 49, 7188−7196

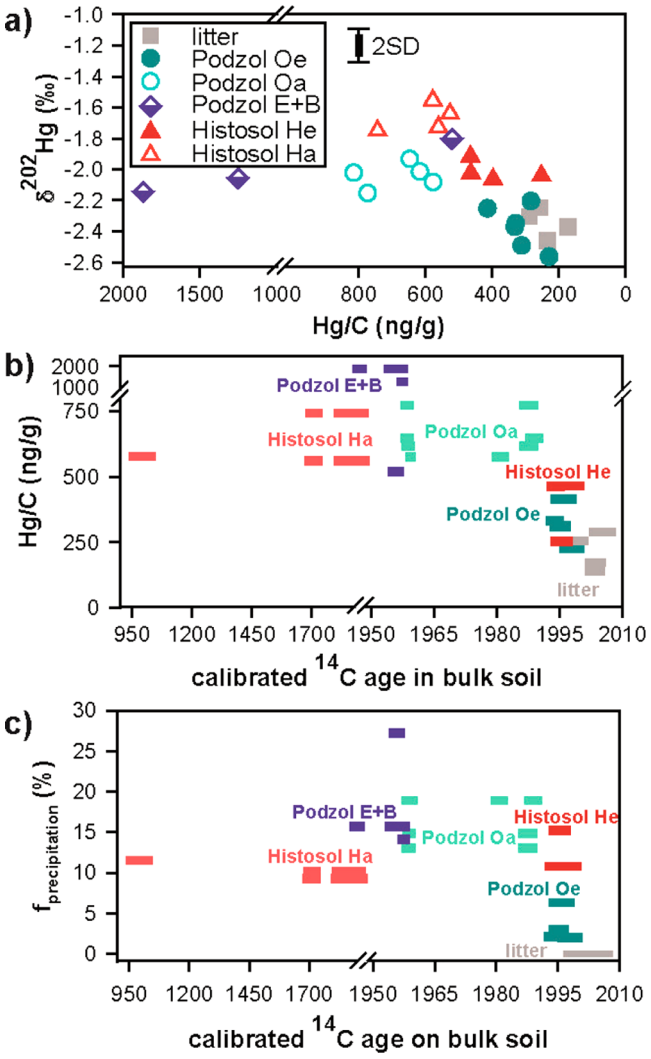

Figure 4. Time dependence of Hg isotope signatures in soil: (a) mass-dependent fractionation (δ^{202}Hg) vs Hg/C ratio (b) Hg/C ratio vs calibrated radiocarbon age in bulk soil, and (c) modeled fraction of precipitation-derived Hg from stable Hg isotope signatures vs calibrated radiocarbon age of bulk soil. The width of the bars represents the calibrated age ranges (for certain radiocarbon signatures multiple age ranges are possible as indicated by multiple bars).

variable over time and decreased by about 50% in Scandinavia over the last two decades,[51] potentially affecting the Hg isotope signatures in the soil horizons. Reconstructions of Hg emissions from coal combustion indicate relatively constant Hg isotope signatures over time,[52] and thus do not suggest a direct causal relationship between coal emission signatures and the Hg isotope variations in boreal forest soils reported here. Peat bogs and lake sediments have been used as archives for Hg concentration and isotope composition to record historical atmospheric deposition and anthropogenic contamination.[53,54] However, our results suggest that such archives may be susceptible to overprinting by secondary processes such as reductive Hg losses or accumulation of precipitation-derived Hg. Significant reductive Hg losses from peat bogs might potentially provide an alternative explanation for observed discrepancies between peat and lake sediment archives in the ratio of Hg accumulation rates of preindustrial to modern times.[55,56]

On the basis of the discussion above, the NOM-driven Hg(II) reduction hypothesis appears to be the most plausible explanation for the observed Hg isotope signatures in the Histosol samples. Nonphotochemical abiotic reduction of Hg(II) by NOM has been previously observed in laboratory experiments.[6−8] NOM plays a dual role in Hg redox reactions; on the one hand providing electrons, but on the other hand decreasing rates of Hg(II) reduction and Hg(0) evasion by strong complexation to organic thiol groups and reoxidation.[8] Together with previously missing evidence for NOM-driven Hg(II) reduction under natural conditions, this led to ambiguity about the importance of the process for global Hg cycling.[7] The remarkable correlation between the δ^{202}Hg and Δ^{199}Hg values of Histosol samples and the theoretical NOM-reduction trajectory (R^2 =0.65, Figure 3a) suggests that NOM reduction may be an important process in boreal forest soils. Recent measurements of interstitial soil air, exhibiting the highest Hg(0) concentrations in organic-rich soil layers at high temperatures and low redox potentials,[57] provide further support for this hypothesis.

Reductive Hg Re-emission Fluxes. Using the isotopic enrichment factor for NOM-driven reduction,[9] we calculated reductive Hg losses for soil samples which could not be described by a mixing of litter- and precipitation-derived Hg. The calculated loss for Histosol Ha horizons was between 24% and 33% (average 28%) of the total previously deposited Hg (Figure 5, SI Table S10). For the Histosol He sample which could not be explained by the mixing scenarios for litter- and precipitation-derived Hg (Histosol-He-4), a reductive Hg loss of 12% was calculated. The isotopic enrichment factor reported for microbial reduction ($\varepsilon^{202}Hg_{product/reactant}$= −0.4‰)[10] is much smaller than that for NOM-driven reduction ($\varepsilon^{202}Hg_{product/reactant}$= −1.5‰).[9] Therefore, assuming an important contribution of microbial reduction would result in even higher reductive Hg losses (SI Figure S8, Table S9). For indirect microbial Hg(II) reduction, using NOM as electron shuttle, we would expect a Hg isotope fractionation trajectory following the NOM-driven reduction.[9] Considering the Hg pool sizes in the soil horizons and the radiocarbon age, a reductive loss of 28% in Histosol Ha horizons corresponds to a calculated Hg re-emission flux of 2.2 μg m^{-2} yr^{-1} (Figure 5). If reductive re-emission from the He horizons is also included, then Histosols are expected to exhibit re-emission fluxes of ∼5 μg m^{-2} yr^{-1}. These estimates based on Hg isotope signatures and radiocarbon ages, integrating over the entire history of the soil horizons, are higher but on the same order of magnitude as compared to estimates based on the extrapolation of Hg flux measurements from forest soils.[5,58]

Implications for Global Hg Cycling. Global models suggest that ∼60% of today's Hg deposition originates from re-emitted legacy anthropogenic Hg, making Hg re-emission from terrestrial surfaces one of the major sources of Hg emissions to the atmosphere.[3] Current global Hg models account for Hg evasion from soils by coupling the Hg loss to carbon respiration in soils, based on empirical correlations between Hg and C observed in some studies.[2,3] However, large uncertainties exist concerning the long-term storage of Hg in soils and terrestrial re-emission rate coefficients.[59,60] Our data suggest that poorly drained Histosols exhibit significant reductive Hg re-emission rates, despite being characterized by high carbon accumulation rates. This finding indicates a higher mobility of Hg in reducing environments than previously suggested. The significant Hg re-emission upon reduction reported here clearly reveals the

DOI: 10.1021/acs.est.5b00742
Environ. Sci. Technol. 2015, 49, 7188−7196

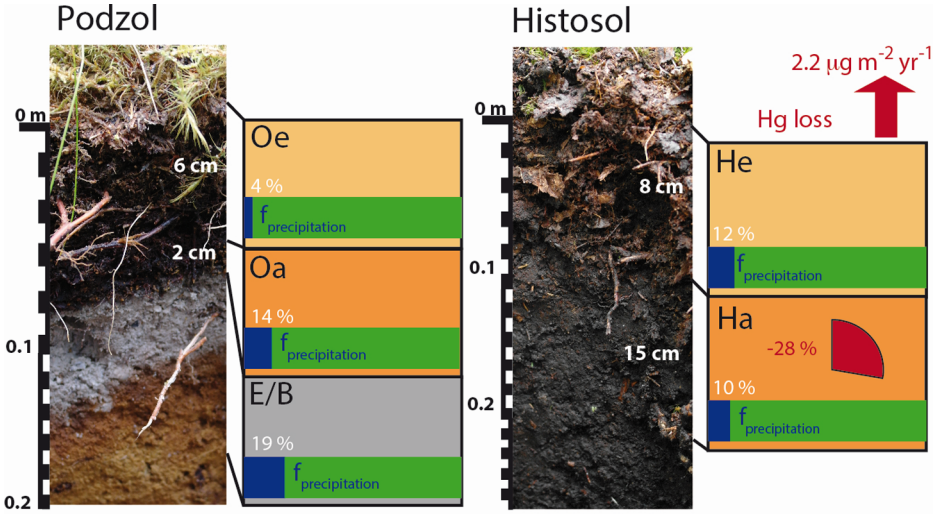

Figure 5. Summary of modeled results of different soil types (Podzols and Histosols): Fraction of precipitation-derived Hg ($f_{precipitation}$ as % of total Hg, the rest corresponds to litter-derived Hg) and modeled Hg loss by nonphotochemical abiotic reduction by natural organic matter.

limitations of the coupling approach of Hg to C used in global Hg models.[2,3] No dependence of Hg dynamics on C mineralization was observed in a recent study, suggesting Hg(0) immobilization in mineral soils.[39] We anticipate that with higher temperatures and precipitation at northern latitudes, driven by global warming leading to generally more anoxic conditions in peatlands and a melting of permafrost,[51] Hg reduction and subsequently Hg re-emission from organic soils will increase. Therefore, we demonstrate the need for a process-based ecosystem-specific assessment of Hg re-emissions to improve predictions of future global Hg cycling. Stable Hg isotope approaches as applied in this study can be an important tool in this future research direction and provide new insights into the mechanisms and fluxes associated with land/atmosphere exchange of Hg.

■ ASSOCIATED CONTENT

Supporting Information

Additional method details, figures, and tables. The Supporting Information is available free of charge on the ACS Publications website at DOI: 10.1021/acs.est.5b00742.

■ AUTHOR INFORMATION

Corresponding Authors

*E-mail: martin.jiskra@get.obs-mip.fr (M.J.).
*Phone: +41-44-6336008; fax: +41-44-6331118; e-mail: wiederhold@env.ethz.ch (J.G.W.).

Present Address

[⊥]Laboratoire Géosciences Environnement Toulouse, Observatoire Midi-Pyrénées, CNRS-IRD-Université Paul Sabatier, 31062 Toulouse, France.

Notes

The authors declare no competing financial interest.

■ ACKNOWLEDGMENTS

We would like to thank Kurt Barmettler for his support in the soil chemistry laboratory and Colin Maden and Robin Smith for assistance in the isotope geochemistry laboratory. We are grateful to Urs Menet, Donat Niederer, Daniel Schnarwiler, and Andreas Suesli for their help with manufacturing the two-stage combustion oven. We thank Alexander Brunner, Christa Bodmer, and Alexandra Metzger for help with sample preparation and concentration analyses and Marita Skarpeli-Liati for field assistance. We acknowledge Daniel Obrist, Jeroen Sonke, and Bernard Bourdon for helpful discussions, Jeroen Sonke and JiuBin Chen for sharing prepublication data, and four anonymous reviewers for helpful comments. This research was funded by ETH Zurich (Grant ETH-1509-2) and the Swedish Research Council for Environment and Spatial Planning (FORMAS, no. 29-2009-1207).

■ REFERENCES

(1) Mason, R. P.; Choi, A. L.; Fitzgerald, W. F.; Hammerschmidt, C. R.; Lamborg, C. H.; Soerensen, A. L.; Sunderland, E. M. Mercury biogeochemical cycling in the ocean and policy implications. *Environ. Res.* **2012**, *119*, 101−117.

(2) Smith-Downey, N. V.; Sunderland, E. M.; Jacob, D. J. Anthropogenic impacts on global storage and emissions of mercury from terrestrial soils: Insights from a new global model. *J. Geophys. Res.-Biogeosci.* **2010**, *115*, G03008.

(3) Amos, H. M.; Jacob, D. J.; Streets, D. G.; Sunderland, E. M. Legacy impacts of all-time anthropogenic emissions on the global mercury cycle. *Global Biogeochem. Cycl.* **2013**, *27*, 410−421.

(4) Driscoll, C. T.; Mason, R. P.; Chan, H. M.; Jacob, D. J.; Pirrone, N. Mercury as a global pollutant: sources, pathways, and effects. *Environ. Sci. Technol.* **2013**, *47*, 4967−4983.

(5) Denkenberger, J. S.; Driscoll, C. T.; Branfireun, B. A.; Eckley, C. S.; Cohen, M.; Selvendiran, P. A synthesis of rates and controls on elemental mercury evasion in the Great Lakes Basin. *Environ. Pollut.* **2012**, *161*, 291−298.

(6) Alberts, J. J.; Schindle, J. E.; Miller, R. W.; Nutter, D. E. Elemental mercury evolution mediated by humic acid. *Science* **1974**, *184*, 895−896.

(7) Gu, B.; Bian, Y.; Miller, C. L.; Dong, W.; Jiang, X.; Liang, L. Mercury reduction and complexation by natural organic matter in anoxic environments. *Proc. Natl. Acad. Sci. U.S.A.* **2011**, *108*, 1479−1483.

(8) Jiang, T.; Skyllberg, U.; Wei, S.; Wang, D.; Lu, S.; Jiang, Z.; Flanagan, D. C. Modeling of the structure-specific kinetics of abiotic, dark reduction of Hg(II) complexed by O/N and S functional groups in humic acids while accounting for time-dependent structural rearrangement. *Geochim. Cosmochim. Acta* **2015**, *154*, 151−167.

(9) Zheng, W.; Hintelmann, H. Nuclear field shift effect in isotope fractionation of mercury during abiotic reduction in the absence of light. *J. Phys. Chem. A* **2010**, *114*, 4238−4245.

DOI: 10.1021/acs.est.5b00742
Environ. Sci. Technol. 2015, 49, 7188−7196

(10) Kritee, K.; Blum, J. D.; Johnson, M. W.; Bergquist, B. A.; Barkay, T. Mercury stable isotope fractionation during reduction of Hg(II) to Hg(0) by mercury resistant microorganisms. *Environ. Sci. Technol.* **2007**, *41*, 1889−1895.
(11) Bergquist, B. A.; Blum, J. D. Mass-dependent and -independent fractionation of Hg isotopes by photoreduction in aquatic systems. *Science* **2007**, *318*, 417−420.
(12) Grigal, D. F.; Kolka, R. K.; Fleck, J. A.; Nater, E. A. Mercury budget of an upland-peatland watershed. *Biogeochem.* **2000**, *50*, 95−109.
(13) Demers, J. D.; Driscoll, C. T.; Fahey, T. J.; Yavitt, J. B. Mercury cycling in litter and soil in different forest types in the Adirondack region, New York, USA. *Ecol. Appl.* **2007**, *17*, 1341−1351.
(14) Pokharel, A. K.; Obrist, D. Fate of mercury in tree litter during decomposition. *Biogeosci.* **2011**, *8*, 2507−2521.
(15) Wiederhold, J. G. Metal stable isotope signatures as tracers in environmental geochemistry. *Environ. Sci. Technol.* **2015**, *49*, 2606−2624.
(16) Demers, J. D.; Blum, J. D.; Zak, D. R. Mercury isotopes in a forested ecosystem: Implications for air−surface exchange dynamics and the global mercury cycle. *Global Biogeochem. Cycles* **2013**, *27*, 222−238.
(17) Zhang, H.; Yin, R. S.; Feng, X. B.; Sommar, J.; Anderson, C. W.; Sapkota, A.; Fu, X. W.; Larssen, T. Atmospheric mercury inputs in montane soils increase with elevation: evidence from mercury isotope signatures. *Sci. Rep.* **2013**, *3*, 3322.
(18) Zheng, W.; Hintelmann, H. Isotope fractionation of mercury during its photochemical reduction by low-molecular-weight organic compounds. *J. Phys. Chem. A* **2010**, *114*, 4246−4253.
(19) Sherman, L. S.; Blum, J. D.; Johnson, K. P.; Keeler, G. J.; Barres, J. A.; Douglas, T. A. Mass-independent fractionation of mercury isotopes in Arctic snow driven by sunlight. *Nat. Geosci.* **2010**, *3*, 173−177.
(20) *Soil Atlas of the Northern Circumpolar Region*; European Commission, Office of the Official Publications of the European Communities: Luxemburg, 2010.
(21) Jiskra, M.; Wiederhold, J. G.; Bourdon, B.; Kretzschmar, R. Solution speciation controls mercury isotope fractionation of Hg(II) sorption to goethite. *Environ. Sci. Technol.* **2012**, *46*, 6654−6662.
(22) Smith, R. S.; Wiederhold, J. G.; Jew, A. D.; Brown, G. E., Jr; Bourdon, B.; Kretzschmar, R. Small-scale studies of roasted ore waste reveal extreme ranges of stable mercury isotope signatures. *Geochim. Cosmochim. Acta* **2014**, *137*, 1−17.
(23) Smith, R. S.; Wiederhold, J. G.; Jew, A. D.; Brown, G. E., Jr.; Bourdon, B.; Kretzschmar, R. Stable Hg isotope signatures in creek sediments impacted by a former Hg mine. *Environ. Sci. Technol.* **2015**, *49*, 767−776.
(24) Chandan, P.; Ghosh, S.; Bergquist, B. A. Mercury isotope fractionation during aqueous photoreduction of monomethylmercury in the presence of dissolved organic matter. *Environ. Sci. Technol.* **2015**, *49*, 259−267.
(25) Wiederhold, J. G.; Skyllberg, U.; Drott, A.; Jiskra, M.; Jonsson, S.; Björn, E.; Bourdon, B.; Kretzschmar, R. Mercury isotope signatures in contaminated sediments as tracer for local industrial pollution sources. *Environ. Sci. Technol.* **2015**, *49*, 177−185.
(26) Wacker, L.; Bonani, G.; Friedrich, M.; Hajdas, I.; Kromer, B.; Nemec, M.; Ruff, M.; Suter, M.; Synal, H. A.; Vockenhuber, C. MICADAS: routine and high-precision radiocarbon dating. *Radiocarbon* **2010**, *52*, 252−262.
(27) Stuiver, M.; Polach, H. A. Reporting of C-14 data—discussion. *Radiocarbon* **1977**, *19*, 355−363.
(28) Reimer, P. J.; Brown, T. A.; Reimer, R. W. Discussion: Reporting and calibration of post-bomb C-14 data. *Radiocarbon* **2004**, *46*, 1299−1304.
(29) Reimer, P. J.; Bard, E.; Bayliss, A.; Beck, J. W.; Blackwell, P. G.; Ramsey, C. B.; Buck, C. E.; Cheng, H.; Edwards, R. L.; Friedrich, M.; Grootes, P. M.; Guilderson, T. P.; Haflidason, H.; Hajdas, I.; Hatte, C.; Heaton, T. J.; Hoffmann, D. L.; Hogg, A. G.; Hughen, K. A.; Kaiser, K. F.; Kromer, B.; Manning, S. W.; Niu, M.; Reimer, R. W.; Richards, D. A.; Scott, E. M.; Southon, J. R.; Staff, R. A.; Turney, C. S. M.; van der Plicht, J. INTCAL13 and MARINE13 radiocarbon age calibration curves 0−50 000 years cal BP. *Radiocarbon* **2013**, *55*, 1869−1887.
(30) Hua, Q.; Barbetti, M.; Rakowski, A. Z. Atmospheric radiocarbon for the period 1950−2010. *Radiocarbon* **2013**, *55*, 2059−2072.
(31) Gratz, L. E.; Keeler, G. J.; Blum, J. D.; Sherman, L. S. Isotopic composition and fractionation of mercury in great lakes precipitation and ambient air. *Environ. Sci. Technol.* **2010**, *44*, 7764−7770.
(32) Chen, J. B.; Hintelmann, H.; Feng, X. B.; Dimock, B. Unusual fractionation of both odd and even mercury isotopes in precipitation from Peterborough, ON, Canada. *Geochim. Cosmochim. Acta* **2012**, *90*, 33−46.
(33) Sherman, L. S.; Blum, J. D.; Keeler, G. J.; Demers, J. D.; Dvonch, J. T. Investigation of local mercury deposition from a coal-fired power plant using mercury isotopes. *Environ. Sci. Technol.* **2012**, *46*, 382−390.
(34) Donovan, P. M.; Blum, J. D.; Yee, D.; Gehrke, G. E.; Singer, M. B. An isotopic record of mercury in San Francisco bay sediment. *Chem. Geol.* **2013**, *349*, 87−98.
(35) Fu, X.; Heimburger, L.-E.; Sonke, J. E. Collection of atmospheric gaseous mercury for stable isotope analysis using iodine- and chlorine-impregnated activated carbon traps. *J. Anal. At. Spectrom.* **2014**, *29*, 841−852.
(36) Wang, Z.; Chen, J.; Feng, X.; Hintelmann, H.; Yuan, S.; Cai, H.; Huang, Q.; Wang, S. Mass-dependent and mass-independent fractionation of mercury isotopes in precipitation from Guiyang, SW China. *C. R. Geosci.* DOI: 10.1016/j.crte.2015.02.006.
(37) Alriksson, A. Regional variability of Cd, Hg, Pb, and C concentrations in different horizons of Swedish forest soils. *Water Air Soil Pollut.* **2001**, *1*, 325−341.
(38) Blum, J. D.; Sherman, L. S.; Johnson, M. W. Mercury isotopes in earth and environmental sciences. *Annu. Rev. Earth Planet. Sci.* **2014**, *42*, 249−269.
(39) Obrist, D.; Pokharel, A. K.; Moore, C. Vertical profile measurements of soil air suggest immobilization of gaseous elemental mercury in mineral soil. *Environ. Sci. Technol.* **2014**, *48*, 2242−2252.
(40) Biswas, A.; Blum, J. D.; Bergquist, B. A.; Keeler, G. J.; Xie, Z. Q. Natural mercury isotope variation in coal deposits and organic soils. *Environ. Sci. Technol.* **2008**, *42*, 8303−8309.
(41) St Louis, V. L.; Rudd, J. W. M.; Kelly, C. A.; Hall, B. D.; Rolfhus, K. R.; Scott, K. J.; Lindberg, S. E.; Dong, W. Importance of the forest canopy to fluxes of methyl mercury and total mercury to boreal ecosystems. *Environ. Sci. Technol.* **2001**, *35*, 3089−3098.
(42) Graydon, J. A.; St Louis, V. L.; Lindberg, S. E.; Sandilands, K. A.; Rudd, J. W.; Kelly, C. A.; Harris, R.; Tate, M. T.; Krabbenhoft, D. P.; Emmerton, C. A.; Asmath, H.; Richardson, M. The role of terrestrial vegetation in atmospheric Hg deposition: Pools and fluxes of spike and ambient Hg from the METAALICUS experiment. *Glob. Biogeochem. Cycles* **2012**, *26*, GB1022.
(43) Blackwell, B. D.; Driscoll, C. T. Deposition of mercury in forests along a montane elevation gradient. *Environ. Sci. Technol.* **2015**, DOI: 10.1021/es505928w.
(44) Obrist, D.; Johnson, D. W.; Lindberg, S. E.; Luo, Y.; Hararuk, O.; Bracho, R.; Battles, J. J.; Dail, D. B.; Edmonds, R. L.; Monson, R. K.; Ollinger, S. V.; Pallardy, S. G.; Pregitzer, K. S.; Todd, D. E. Mercury distribution across 14 US forests. Part I: Spatial patterns of concentrations in biomass, litter, and soils. *Environ. Sci. Technol.* **2011**, *45*, 3974−3981.
(45) Laudon, H.; Berggren, M.; Agren, A.; Buffam, I.; Bishop, K.; Grabs, T.; Jansson, M.; Kohler, S. Patterns and dynamics of dissolved organic carbon (DOC) in boreal streams: The role of processes, connectivity, and scaling. *Ecosystems* **2011**, *14*, 880−893.
(46) Jiskra, M. *Terrestrial mercury cycling investigated with stable mercury isotopes*; ETH Zurich, PhD dissertation No. 22330, 2014.
(47) Fritsche, J.; Obrist, D.; Alewell, C. Evidence of microbial control of Hg-0 emissions from uncontaminated terrestrial soils. *J. Plant Nutr. Soil Sci.* **2008**, *171*, 200−209.
(48) Poulain, A. J.; Ni Chadhain, S. M.; Ariya, P. A.; Amyot, M.; Garcia, E.; Campbell, P. G. C.; Zylstra, G. J.; Barkay, T. Potential for

DOI: 10.1021/acs.est.5b00742
Environ. Sci. Technol. 2015, 49, 7188−7196

mercury reduction by microbes in the high arctic. *Appl. Environ. Microbiol.* **2007**, *73*, 2230−2238.
(49) Wiederhold, J. G.; Cramer, C. J.; Daniel, K.; Infante, I.; Bourdon, B.; Kretzschmar, R. Equilibrium mercury isotope fractionation between dissolved Hg(II) species and thiol-bound Hg. *Environ. Sci. Technol.* **2010**, *44*, 4191−4197.
(50) Deming, W. E. *Statistical Adjustment of Data*; John Wiley& Sons: New York, 1943.
(51) Rydberg, J.; Klaminder, J.; Rosen, P.; Bindler, R. Climate driven release of carbon and mercury from permafrost mires increases mercury loading to sub-arctic lakes. *Sci. Total Environ.* **2010**, *408*, 4778−4783.
(52) Sun, R.; Sonke, J. E.; Heimburger, L. E.; Belkin, H. E.; Liu, G.; Shome, D.; Cukrowska, E.; Liousse, C.; Pokrovsky, O. S.; Streets, D. G. Mercury stable isotope signatures of world coal deposits and historical coal combustion emissions. *Environ. Sci. Technol.* **2014**, *48*, 7660−7668.
(53) Shotyk, W.; Goodsite, M. E.; Roos-Barraclough, F.; Frei, R.; Heinemeier, J.; Asmund, G.; Lohse, C.; Hansen, T. S. Anthropogenic contributions to atmospheric Hg, Pb and As accumulation recorded by peat cores from southern Greenland and Denmark dated using the 14C "bomb pulse curve". *Geochim. Cosmochim. Acta* **2003**, *67*, 3991−4011.
(54) Biester, H.; Bindler, R.; Martinez-Cortizas, A.; Engstrom, D. R. Modeling the past atmospheric deposition of mercury using natural archives. *Environ. Sci. Technol.* **2007**, *41*, 4851−4860.
(55) Engstrom, D. R.; Fitzgerald, W. F.; Cooke, C. A.; Lamborg, C. H.; Drevnick, P. E.; Swain, E. B.; Balogh, S. J.; Halcom, P. H. Atmospheric Hg emissions from preindustrial gold and silverextraction in the Americas: A reevaluation from lake-sediment archives. *Environ. Sci. Technol.* **2014**, *58*, 6533−6543.
(56) Amos, H. M.; Sonke, J. E.; Obrist, D.; Robins, N.; Hagan, N.; Horowitz, H. M.; Mason, R.; Witt, M.; Hedgecock, I. M.; Corbitt, E. S.; Sunderland, E. M. Observational and modeling constraints on global anthropogenic enrichment of mercury. *Environ. Sci. Technol.* **2015**, *49*, 4036−4047.
(57) Moore, C. W.; Castro, M. S. Investigation of factors affecting gaseous mercury concentrations in soils. *Sci. Total Environ.* **2012**, *419*, 136−143.
(58) Lindberg, S. E.; Hanson, P. J.; Meyers, T. P.; Kim, K. H. Air/surface exchange of mercury vapor over forests—The need for a reassessment of continental biogenic emissions. *Atmos. Environ.* **1998**, *32*, 895−908.
(59) Amos, H. M.; Jacob, D. J.; Kocman, D.; Horowitz, H. M.; Zhang, Y.; Dutkiewicz, S.; Horvat, M.; Corbitt, E. S.; Krabbenhoft, D. P.; Sunderland, E. M. Global biogeochemical implications of mercury discharges from rivers and sediment burial. *Environ. Sci. Technol.* **2014**, *48*, 9514−9522.
(60) Horowitz, H. M.; Jacob, D. J.; Amos, H. M.; Streets, D. G.; Sunderland, E. M. Historical mercury releases from commercial products: Global environmental implications. *Environ. Sci. Technol.* **2014**, *48*, 10242−10250.

DOI: 10.1021/acs.est.5b00742
Environ. Sci. Technol. 2015, 49, 7188−7196